



Original Research

Photoimmunotheranostics of epithelioid sarcoma by targeting CD44 or EGFR

Jiefu Jin^{a, **}, James D. Barnett^a, Yelena Mironchik^a, John Gross^d, Hisataka Kobayashi^f, Adam Levin^e, Zaver M. Bhujwalla^{a, b, c, *}

^a Division of Cancer Imaging Research, The Russell H Morgan Department of Radiology and Radiological Science, The Johns Hopkins University School of Medicine, Baltimore, MD, USA

^b Sidney Kimmel Comprehensive Cancer Center, The Johns Hopkins University School of Medicine, Baltimore, MD, USA

^c Department of Radiation Oncology and Molecular Radiation Sciences, The Johns Hopkins University School of Medicine, Baltimore, MD, USA

^d Department of Pathology, The Johns Hopkins University School of Medicine, Baltimore, MD, USA

^e Orthopaedic Oncology, The Johns Hopkins University School of Medicine, Baltimore, MD, USA

^f Laboratory of Molecular Theranostics, Molecular Imaging Branch, NCI/NIH, Bethesda, MD, USA

ARTICLE INFO

Keywords:

Epithelioid sarcoma
Photoimmunotheranostics
CD44
EGFR
Targeted therapy

ABSTRACT

Epithelioid sarcoma (ES) is a rare soft tissue neoplasm with high recurrence rates. Wide surgical resection remains the only potential curative treatment. ES presents most commonly on the fingers, hands and forearm, making light-based cancer cell-targeted therapies such as near-infrared photoimmunotherapy (NIR-PIT) that is target-specific, but with limited penetration depth, suitable for ES treatment. We established that CD44 and EGFR were overexpressed in ES patient samples and in the VA-ES-BJ human ES cell line. NIR-PIT of VA-ES-BJ cells using antibody photosensitizer conjugates, prepared by conjugating a CD44 or EGFR monoclonal antibody to the photosensitizer IR700, confirmed that NIR-PIT with both conjugates resulted in cell death. Neither treatment with NIR light alone nor treatment with the conjugates but without NIR light were effective. CD44-IR700-PIT resulted in greater cell death than EGFR-IR700-PIT, consistent with the increased expression of CD44 by VA-ES-BJ cells. In tumors, EGFR-IR700 exhibited a higher tumor-to-normal ratio, as determined by in vivo fluorescence imaging, and a higher anti-tumor growth effect, compared to CD44-IR700. No antitumor effect of the EGFR antibody or the photosensitizer conjugate alone was observed in vivo. Our data support evaluating the use of EGFR-IR700-PIT in the management of ES for detecting and eliminating ES cells in surgical margins, and in the treatment of superficial recurrent tumors.

Introduction

First identified by Enzinger in 1970 [1], epithelioid sarcoma (ES) is a slow-growing malignant soft tissue sarcoma (STS) [2]. Although ES is a rare malignancy comprising approximately 1–1.4 % of all STSs [3], it is one of the most common STSs in the hand and the upper limb [4]. Different from other STSs, ES has high local recurrence (LR), and a high

frequency of lymphatic spread with an overall poor prognosis [5]. The overall rates of recurrence and metastasis of ES are 63 % and 42 %, respectively, and the overall 5- and 10-year survival rates of ES are 60 % and 49 %, respectively [6].

ES treatments vary depending on the tumor stage, the patient's functional status after resection, and margin assessment [4]. For low-grade and resectable high-grade ES, wide surgical resection remains

Abbreviations: ATCC, American type culture collection; CEA, carcinoembryonic antigen; EGFR, epidermal growth factor receptor; ES, epithelioid sarcoma; H&E, hematoxylin and eosin; Her2, human epidermal growth factor receptor-2; IHC, immunohistochemistry; INI1, integrase interactor 1; IR700, IRDye700DX; LED, light emitting diode; LR, local recurrence; MFI, mean fluorescence intensity, NCCN, national comprehensive cancer network; NIR-PIT, near-infrared photoimmunotherapy; OS, overall survival; PFS, progression-free survival; p.i., post injection; PMDA, pharmaceuticals and medical devices agency; PSMA, prostate-specific membrane antigen; RIPA, radioimmune precipitation; ROIs, regions of interest; RT, radiation therapy; SD, standard deviation; STS, soft tissue sarcoma.

* Corresponding author at: Division of Cancer Imaging Research, Department of Radiology, Johns Hopkins University School of Medicine, Rm 208C Traylor Bldg., 720 Rutland Avenue, Baltimore, MD 21205, USA.

** Corresponding author.

E-mail addresses: jjin@jhmi.edu (J. Jin), zbhujwa1@jhmi.edu (Z.M. Bhujwalla).

<https://doi.org/10.1016/j.tranon.2024.101966>

Received 25 August 2023; Received in revised form 5 April 2024; Accepted 16 April 2024

1936-5233/© 2024 Published by Elsevier Inc. This is an open access article under the CC BY-NC-ND license (<http://creativecommons.org/licenses/by-nc-nd/4.0/>).

the only potential curative treatment [8] based on the National Comprehensive Cancer Network (NCCN) STS clinical guidelines (Version 2.2022) [9]. However, in instances where critical structures need to be preserved and wide margins are not possible, surgical resection may result in microscopically positive margins which is a strong predictor of LR [10]. Although radiation therapy (RT) is routinely used when clear margins are not achieved, the benefits of RT are inconsistent in terms of LR rates, overall survival (OS) and progression-free survival (PFS) [6,7,11]. Neoadjuvant or adjuvant systemic chemotherapy is not commonly considered for localized ES due to the unclear benefits [7]. Because of unsatisfactory outcomes and long-term side effects from RT, NCCN STS guidelines strongly recommend re-resection over RT for the management of patients with positive margins, and suggest postoperative RT only if re-resection is not feasible and the patient has not previously received RT [9]. This conservative use of RT identifies an unmet need for the development of new and preferably targeted therapies, to supplement or even replace RT in the management of ES patients with positive margins. For patients with unresectable locally advanced and metastatic ES, the prognosis is poor and anthracycline-based chemotherapy regimens, preferably in combination with ifosfamide, are preferred as a first-line treatment, despite limited and conflicting data regarding the role of chemotherapy [7]. Studies showed that systemic chemotherapy improved OS in the palliative treatment of advanced and metastatic ES [11]. Targeted therapy was unavailable for ES until 2020 when the FDA approved tazemetostat, an EZH2 inhibitor, for the treatment of adults and pediatric patients aged 16 years and older with metastatic or locally advanced epithelioid sarcoma not eligible for margin-negative resection [12–14]. The overall response rate was 15 %, of which 1.6 % of patients had a complete response and 13 % had a partial response. Despite relatively low response rates, tazemetostat was granted accelerated approval and received orphan drug designation from the FDA, highlighting the unmet medical need for targeted therapies of ES.

Near infrared photoimmunotherapy (NIR-PIT) is an emerging targeted cancer therapy that employs a water-soluble and photo-stable phthalocyanine dye IRDye700DX (IR700) as a photosensitizer and an antibody as the targeting moiety [15]. The antibody-photosensitizer conjugate binds to its target on cancer cells [15] or stromal [16] or immune cells [17], and the subsequent NIR light exposure results in damage to the cell membrane and cell death [18]. An international multicenter randomized phase 3 clinical trial of NIR-PIT using cetuximab-IR700 (ASP-1929) to treat recurrent head and neck cancer patients who have failed at least two lines of therapy is on-going (<https://clinicaltrials.gov/ct2/show/NCT03769506>) [19]. In September 2020, the first drug and laser system for human use, cetuximab-IR700 (ASP-1929, Akalux™) and a 690 nm laser system (BioBlade™), were conditionally approved and registered for clinical use by the Pharmaceuticals and Medical Devices Agency (PMDA) in Japan, with health insurance coverage available for recurrent head and neck squamous cell carcinoma since January 2021.

Similar to RT, NIR-PIT requires tumor localized light delivery. However, unlike RT, target-specific cell death occurs only when antibody binding and light exposure are combined. Several cancer targets have been investigated with NIR-PIT, including epidermal growth factor receptor (EGFR) [15,20–24], human epidermal growth factor receptor-2 (Her2) [25,26], prostate-specific membrane antigen (PSMA) [27], carcinoembryonic antigen (CEA) [28,29], CD44 [30], PD-L1 [31,32], Gr1 [33], and fibroblast activation protein- α (FAP- α) [16,34,35]. These studies have been performed with head and neck [15], lung [21,25,26,32], gastric [29], brain [24], prostate [27,32], pancreatic [28,36], breast [20,22,30,34], ovarian [23,31], and esophageal [16,35] cancers. Here, for the first time, we have investigated its use in the management of ES. CD44 plays an important role in tumor progression in many cancers of epithelial origin [37,38]. In a recent review, a high expression of CD44 was identified in STS supporting the possibility that it is also expressed by ES [39]. Similarly, enhanced EGFR expression but not

EGFR amplification or gene mutation was identified in a cohort of human ES samples [40]. We therefore focused on CD44 and EGFR for evaluating the use of NIR-PIT for targeted treatment of ES using VA-ES-BJ cells and tumors.

Materials and methods

Reagents

The water soluble phthalocyanine dye, IRDye 700DX NHS ester (IR700) was obtained from Li-Cor Bioscience (Lincoln, NE, USA). Anti-CD44 monoclonal rat IgG2b antibody (clone IM7), rat IgG2b isotype control (clone LTF-2), anti-MUC1 monoclonal mouse IgG3 antibody (clone C595), and anti-EGFR monoclonal mouse IgG1 antibody (clone 225) were purchased from BioXcell (Lebanon, New Hampshire, USA).

Cell culture

A human epithelioid sarcoma cell line, VA-ES-BJ, was purchased from American Type Culture Collection (ATCC, Manassas, VA, USA). Cells were cultured in DMEM medium supplemented with 10 % FBS (Sigma, St. Louis, MO, USA) and were maintained at 37 °C in a humidified atmosphere containing 5 % CO₂.

Synthesis of IR700-conjugated antibodies and concentration determination

The synthesis of IR700-conjugated antibodies was performed as reported previously [30]. Briefly, 1 mg of anti-CD44 or anti-EGFR antibody or isotype control was first dispersed in 1 ml of 1 × PBS containing 159.2 µg of IR700 (81.6 nmol, 1 mM in DMSO). The mixture was kept at 4 °C for overnight, and then loaded onto Amicon Ultra-0.5 10 K cutoff filter units (Millipore, Burlington, MA, USA) to remove the unbound IR700 molecules. The purified and concentrated conjugates denoted as CD44-IR700, EGFR-IR700 and IgG-IR700, were sterilized by filtering through Millex-GV filter with 0.22 µm pore size (Millipore). The concentration of antibody and dye/protein ratio was calculated by measuring the absorbance at 280 nm ($\epsilon_{\text{antibody}} = 210,000 \text{ M}^{-1} \text{ cm}^{-1}$) and 689 nm ($\epsilon_{\text{IR700}} = 165,000 \text{ M}^{-1} \text{ cm}^{-1}$). The correction factor of IR700 at 280 nm was 0.095.

In vitro photoimmunotherapy

VA-ES-BJ cell viability was assayed to evaluate the specificity and effectiveness of CD44-IR700 and EGFR-IR700 for in vitro NIR-PIT. Briefly, cells were seeded onto a 96-well plate at a density of six thousand cells/well and kept overnight. After replenishing the medium with conjugates or controls, cells were further incubated for 1 h at 37 °C. After carefully aspirating and replenishing with fresh medium, cells were exposed to light from a light emitting diode (LED, Marubeni, Tokyo, Japan) that provided continuous NIR irradiation at a peak wavelength of 690 nm. Cell viability was determined after NIR irradiation using the CCK-8 assay (Dojindo, Mashiki, Japan). Cytotoxicity data were expressed as mean \pm standard derivation (SD) from quadruple wells. In the dose-dependence experiment, the concentration of CD44-IR700 ranged from 0.2 to 40 µg/ml at 64 J/cm², while the concentration of EGFR-IR700 ranged from 5 to 20 µg/ml at 8 J/cm². In the light exposure-dependence experiment, the concentration of CD44-IR700 was kept at 5 µg/ml or 10 µg/ml, and EGFR-IR700 was kept at 20 µg/ml. To check the specificity of CD44-IR700 or EGFR-IR700-mediated phototoxicity, unconjugated antibodies and IgG-IR700 were used as controls. In a separate study, cells were kept in the dark by wrapping plates with aluminum foil to determine any toxicity of the conjugates.

Animals and tumor model establishment

All animal studies were conducted under an Animal Care and Use

Committee approved protocol. Tumors were established by inoculating 1×10^6 VA-ES-BJ cells in 0.05 ml of Hanks balanced salt solution bilaterally into the flanks of six to eight-week-old female athymic Balb/c (nu/nu) mice purchased from Charles River (Wilmington, MA, USA).

Flow cytometry

VA-ES-BJ cells were dissociated by using TrypLE (Thermo Fisher Scientific, Waltham, MA, USA) and were dispersed at a concentration of 1×10^6 cells per 100 μ l of FACS buffer made of 1 \times PBS supplemented with 1 % BSA and 2 mM EDTA. In a typical staining, 1 μ g of primary antibody was added to the cell suspension for incubation on ice for 30 min. After three washes, cells were re-dispersed in 100 μ l of FACS buffer with 10 μ l of PE-conjugated IgG secondary antibody (F0105B or F0102B, R&D systems, Minneapolis, MN, USA) and incubated on ice for 30 min. For flow cytometry of tumors, freshly resected tumor tissue was dissociated into a single cell suspension by using a tumor dissociation kit (130-096-730, Miltenyi Biotec, Auburn, CA, USA), according to the manufacturer's protocol. The staining of tumor-dissociated cells was similar to VA-ES-BJ cells except that prior to adding the primary antibody, rat anti-mouse CD16/32 antibody (clone 2.4G2, BD Pharmingen™, San Diego, CA, USA) was added for Fc blocking and a LIVE/DEAD™ Fixable Dead Cell Stain Kit (Thermo Fisher Scientific) was used to identify and distinguish live cells from dead cells. Flow cytometry measurements were conducted on a FACS Calibur (BD Bioscience, Franklin Lakes, NJ, USA) with ten thousand events collected for each measurement and analyzed by FlowJo software (Ashland, OR, USA).

Immunohistochemistry (IHC) study

Human epithelioid sarcoma patient samples were kindly provided by Dr. John Gross in the Department of Pathology at Johns Hopkins. The formalin fixed paraffin embedded (FFPE) tumor tissue slides from 4 cases (10 slides per case) and slides from three VA-ES-BJ tumors were stained for hematoxylin and eosin (H&E) and immunostained for CD44 and EGFR according to standard IHC protocols. An anti-CD44 monoclonal mouse antibody (clone 156-3C11, Cell Signaling, Danvers, MA, USA) and an anti-EGFR monoclonal rat antibody (clone D38B1, Cell Signaling) were used for CD44 and EGFR immunostaining, respectively. H&E and IHC slides were digitally scanned at 40 \times magnification.

Immunoblot assay

Tumor tissue obtained after cryogenic grinding, was lysed in radio-immune precipitation (RIPA, Sigma) buffer and measured by a BCA assay (Thermo Fisher Scientific) for protein concentration. Samples with the same amount of protein loading were fractionated by SDS-PAGE, and transferred to a nitrocellulose membrane. An anti-CD44 monoclonal mouse antibody (clone 8E2, Cell Signaling) and an anti-EGFR monoclonal rat antibody (clone D38B1, Cell Signaling) were used to probe CD44 and EGFR, respectively. GAPDH was used as a loading control.

In vivo, ex vivo fluorescence imaging and bio-distribution studies

NIR fluorescence imaging was performed on a Li-Cor Pearl® Impulse imager (LI-COR Biosciences). Nude mice with bilateral VA-ES-BJ tumors (six tumors per group of three mice) were imaged once tumor volumes reached 100 mm³. In a typical imaging study, 100 μ g of CD44-IR700 or EGFR-IR700 or IgG-IR700 was injected through the tail vein, and the fluorescent images were obtained over a 24-h period at 0, 1 h, 24 h post injection (p.i.). At 24 h p.i., mice were euthanized, and the major organs and tumors resected for ex vivo imaging and to obtain weights. All the fluorescent images were acquired under identical experimental conditions. Regions of interest (ROIs) were selected from the in vivo and ex vivo images and analyzed by Pearl Impulse software (LI-COR Biosciences) to obtain values of fluorescence intensity. Bio-distribution

values of the samples in the tumors and main organs at 24 h p.i. were normalized as % injected dose/g (%ID/g) from three mice per group ($n = 3$).

In vivo PIT

Once tumor volumes reached approximately 100 mm³, VA-ES-BJ tumor-bearing mice were randomly assigned to five groups ($n = 4$ per group) based on the injections and conditions: (i) PBS, no PIT; (ii) EGFR-IR700, no PIT; (iii) IgG-IR700-PIT; (iv) CD44-IR700-PIT; (v) EGFR-IR700-PIT. Mice in each group were injected intravenously (i.v.) with 100 μ g of antibody conjugate or with 100 μ l of PBS on day 0 that was repeated on day 7. In the PIT groups, NIR light exposure at a power of 200 J/cm² was given at 24 h p.i. Mice were monitored over a 3-week period (2-week period for PBS no PIT group) by caliper measurement of tumor diameters on Day 0, 4, 7, 11, 14, 18 and 21. Tumor volume was calculated as length \times width² \times 0.5. At the end of treatment, mice were euthanized and tumors were excised to document tumor size.

Statistical analysis

Values were expressed as mean \pm standard deviation (SD) from at least three samples or mice unless otherwise noted. Statistical analysis was performed with a One-way ANOVA (GraphPad Prism). Values of $P \leq 0.05$ were considered significant, unless otherwise stated.

Results

VA-ES-BJ cells and tumors, and human ES tissue overexpress CD44 and EGFR

Both CD44 and EGFR were overexpressed on the surface of VA-ES-BJ cells, as evident from the flow cytometry measurements (Fig. 1a). CD44 had a flow cytometry peak with a higher mean fluorescence value than EGFR (1137 vs. 49), indicating a higher expression level of CD44. The amount of MUC1 on VA-ES-BJ cells was also measured by flow cytometry and compared with CD44 and EGFR (Fig. S1). Although increased expression of MUC1 was detected, this was less than CD44 and EGFR. Sections obtained from three VA-ES-BJ tumors immunostained for CD44 and EGFR expression confirmed the flow cytometry data as shown in Fig. 1b. Human ES tumor tissue samples resected from four ES patients were stained with H&E and immunostained for CD44 or EGFR (Fig. 1c, d, e). The H&E images showed a characteristic appearance of nodular aggregates of fairly uniform, plump epithelioid cells, with relatively abundant eosinophilic cytoplasm and prominent central zonal necrosis (Fig. 1c), consistent with the characteristic ES histology patterns reported previously [2].

ES cells in all four ES patient samples were positive for CD44 (Fig. 1d). However, CD44 positive staining was not exclusive to ES cells, with neighboring lymphocytes that clustered and resided between ES cells showing even stronger CD44 staining. EGFR staining was mostly present on ES cells (Fig. 1e). ES cells in three out of four ES samples were positive for EGFR.

CD44-IR700 and EGFR-IR700 kill VA-ES-BJ cells in a target specific, concentration and light exposure-dependent manner

IR700 was conjugated to anti-CD44 and anti-EGFR antibodies to obtain CD44-IR700 and EGFR-IR700 conjugates, respectively. PIT studies with VA-ES-BJ cells revealed that the cell death rate was dependent on the concentration of the conjugate (Fig. 2a and d) and light exposure intensity (Fig. 2b and e). The concentration of CD44-IR700 (EC₅₀) required to kill 50 % of VA-ES-BJ cells at 8 J/cm² was between 0.2 and 0.5 μ g/ml (1.33–3.33 nM), while the EC₅₀ value for EGFR-IR700 at 64 J/cm² was around 5 μ g/ml (33.3 nM). The higher EC₅₀ value and the requirement of higher exposure intensity for EGFR-

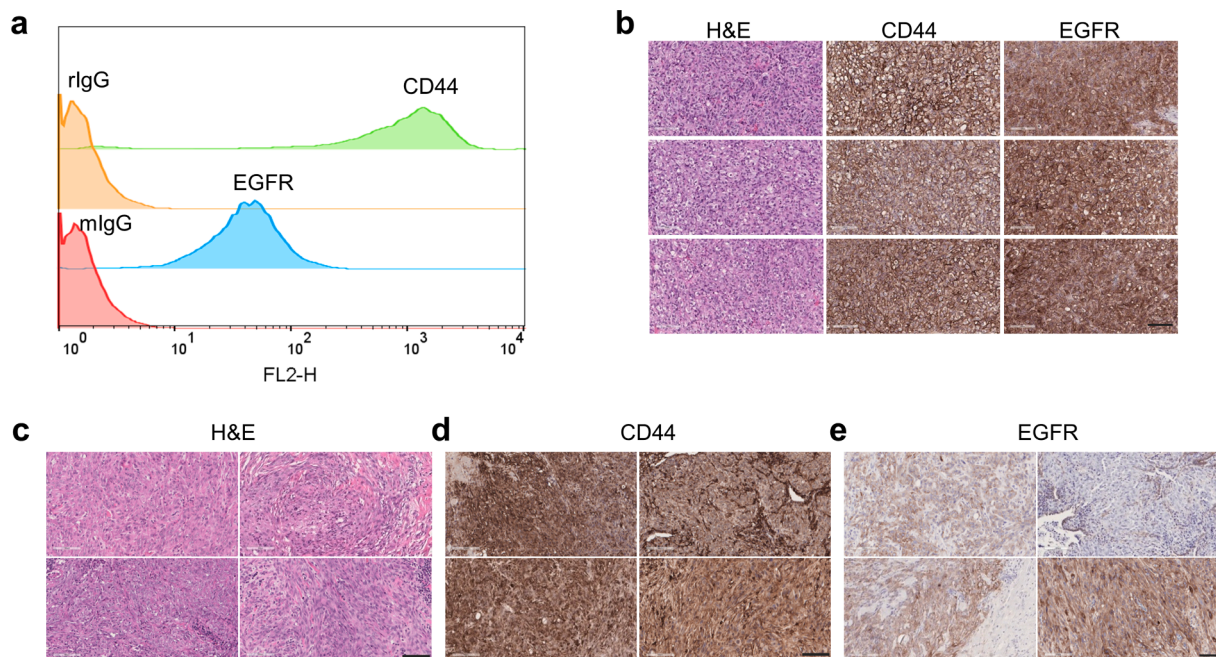


Fig. 1. CD44 and EGFR overexpression in VA-ES-BJ cells and in human ES. (a) The cell surface expression of CD44 and EGFR on VA-ES-BJ cells measured by flow cytometry. The corresponding isotype antibodies were used as controls. (b) Representative images from three VA-ES-BJ xenograft tumor sections after H&E staining (left), immunostaining for CD44 (middle) or EGFR (right) at 20× magnification. Scale bar = 100 μm. Representative images from human ES tumor tissue sections after H&E staining (c), immunostaining for CD44 (d) and EGFR (e) at 20× magnification. Human ES tumor tissue samples were resected from four ES patients. Scale bar = 100 μm.

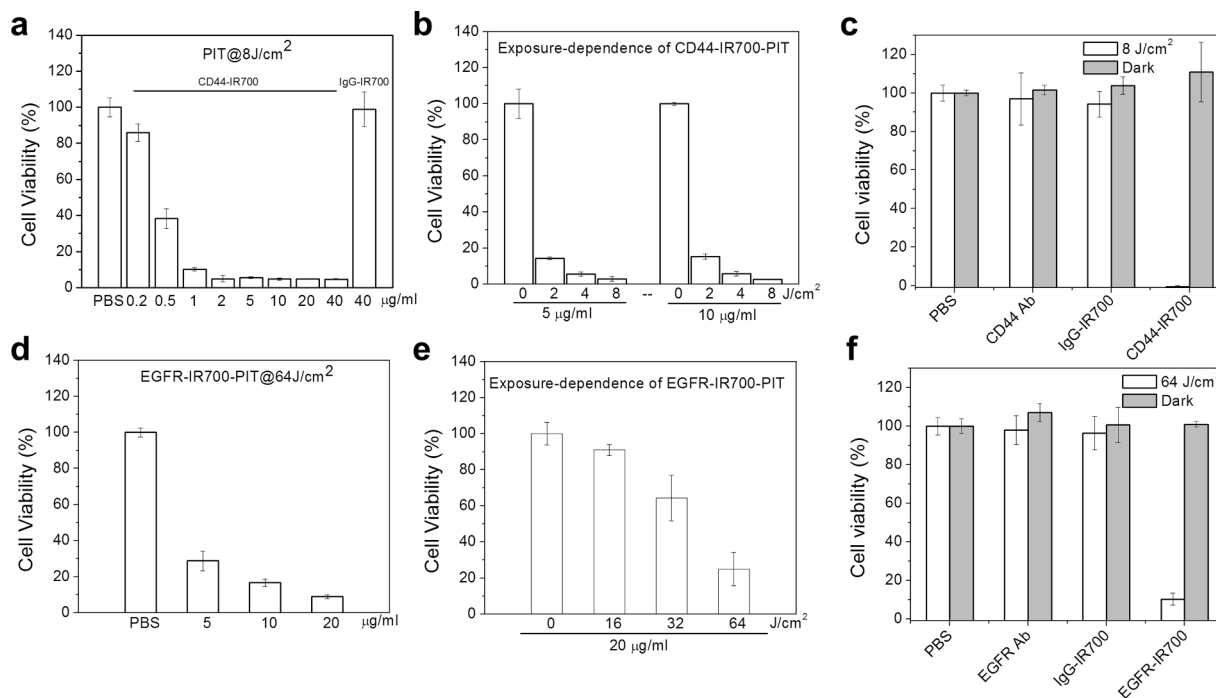


Fig. 2. Concentration and exposure-dependence and target-specific cell death of CD44-IR700 and EGFR-IR700. CD44-IR700-mediated phototoxicity was dependent on the concentration of CD44-IR700 (a) or exposure dose (b). (c) CD44-specific cell death only occurred when VA-ES-BJ cells were exposed to CD44-IR700 and light irradiation. EGFR-IR700-mediated phototoxicity was dependent on the concentration of EGFR-IR700 (d) or exposure dose (e). (f) EGFR-specific cell death only occurred when VA-ES-BJ cells were exposed to both EGFR-IR700 and light irradiation.

IR700 is attributed to the lower expression level of EGFR than CD44 on VA-ES-BJ cells, consistent with the flow cytometry results (Fig. 1a). Both CD44-IR700-PT and EGFR-IR700-PIT were target specific, and the unconjugated antibodies and the conjugates made from isotype antibodies

did not induce cell death in VA-ES-BJ cells (Fig. 2c and f). Under dark conditions, neither CD44-IR700 nor EGFR-IR700 showed any toxicity to VA-ES-BJ cells.

CD44-IR700 and EGFR-IR700 bind preferentially in VA-ES-BJ tumors

Following injection, both CD44-IR700 and EGFR-IR700 were rapidly detected in subcutaneous VA-ES-BJ tumors (Fig. 3a and b). As early as 1 h *p.i.*, a substantial amount of CD44-IR700 or EGFR-IR700 was detected in the tumors with a fluorescence intensity that clearly delineated the tumor. At 24 h *p.i.*, tumor fluorescence in both CD44-IR700 and EGFR-IR700-injected mice was more prominent, and the tumor-to-normal ratio increased as the conjugate cleared from normal tissue. In addition to the tumor and liver, CD44-IR700 was also detected with high intensity in tissues known to have high CD44 expression such as the thymus, bone marrow and spine. For comparison, we ran a control imaging study by injecting an equivalent amount of IgG-IR700 to determine the non-specific uptake of the antibody conjugate. At 24 h *p.i.*, IgG-IR700 was present at a relatively low level in VA-ES-BJ tumors where the tumor was barely identified (Fig. 3c). EGFR-IR700 had a higher tumor-to-normal ratio and a much cleaner background compared to CD44-IR700 and IgG-IR700, especially at 24 h *p.i.* (Fig. 3d). At 24 h *p.i.*, the tumors were resected and measured for fluorescence intensities (Fig. 3e). Tumors in the CD44-IR700 and EGFR-IR700 groups showed much higher mean fluorescence intensity (MFI) than tumors in the IgG-IR700 group (3.9 and 4.8 vs. 1.6), reflecting the selective retention of

CD44-IR700 and EGFR-IR700 in tumors and active binding between the conjugate and its respective target on the tumor cells (Fig. 3f). Quantitative uptake data, obtained from ex vivo fluorescence intensities normalized to the weights of organs and tumors, were presented as the percent injected dose per gram of tissue (%ID/g) (Fig. 3g). At 24 h *p.i.*, both EGFR-IR700 and CD44-IR700 were present in tumors at a higher uptake rate than IgG-IR700 (2.1 % and 3.0 % vs. 0.85 % ID/g). The uptake of EGFR-IR700 in the tumors was the highest (Fig. 3g). The uptake rates of the conjugates in the other main organs were comparable except for higher CD44-IR700 in spleens and lungs (Fig. 3f).

CD44-IR700-PIT and EGFR-IR700-PIT cause growth delay of VA-ES-BJ tumors

CD44-IR700-PIT effectively delayed the growth of VA-ES-BJ tumors (Fig. 4a). The tumor sizes in the CD44-IR700-PIT group were significantly smaller than the PBS group from day 7 to the treatment end, and significantly smaller than the IgG-IR700 group on day 18 (Fig. 4b). EGFR-IR700-PIT had an even more pronounced effect on delaying tumor growth compared to CD44-IR700-PIT, although the differences were not significant until the end of the treatment on day 21 (Fig. 4b). Similar to CD44-IR700-PIT, on day 7, seven days after EGFR-IR700 injection and

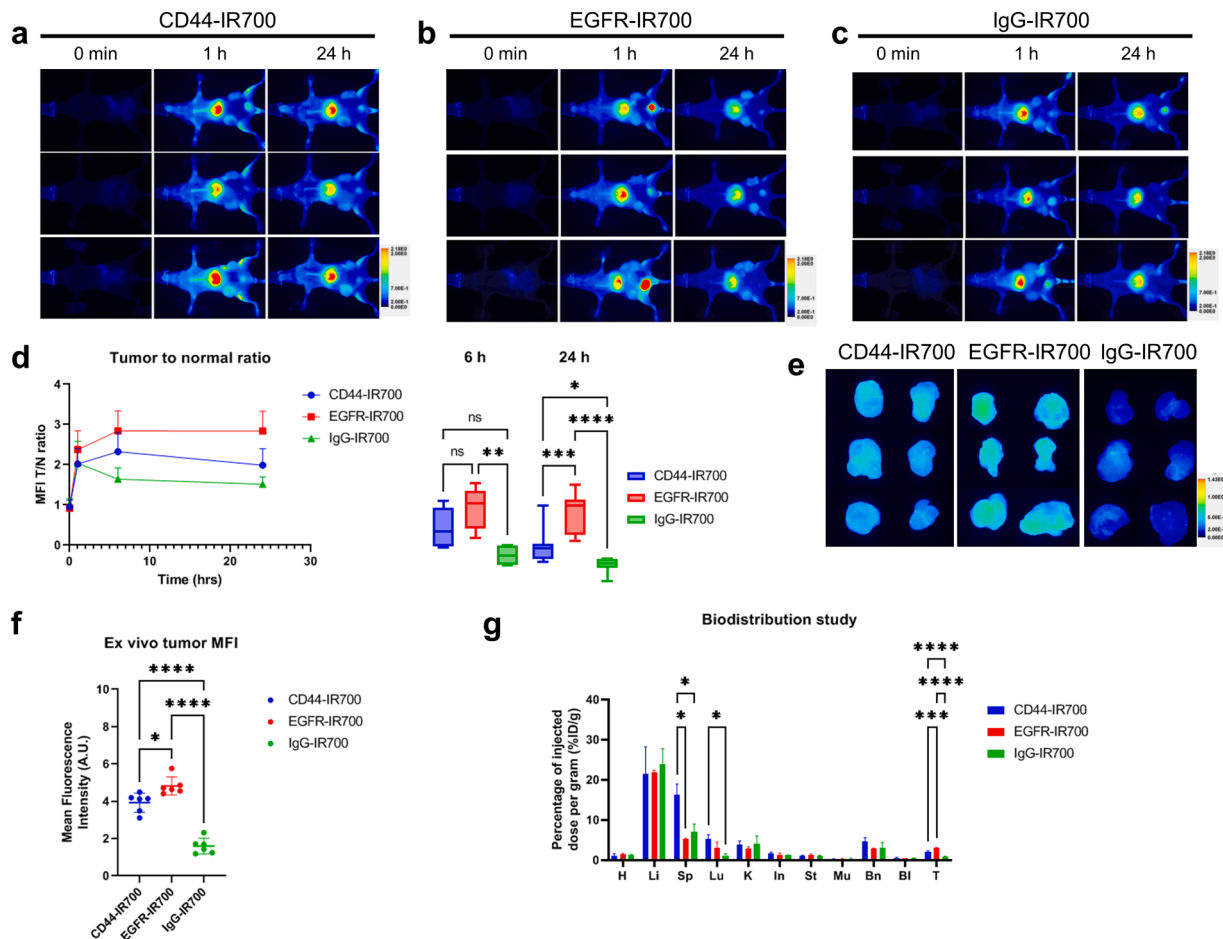


Fig. 3. Preferential accumulation of CD44-IR700 or EGFR-IR700 in VA-ES-BJ tumors. NIR fluorescence imaging of nude mice bearing bilateral VA-ES-BJ tumors over a 24-h period. 100 µg of CD44-IR700 (a) or EGFR-IR700 (b) or IgG-IR700 (c) antibody conjugate was injected *i.v.* (d) Plots of tumor to normal (T/N) ratios measured at 0 min, 1 h, 6 h and 24 h *p.i.* ROIs of tumors and normal tissue were drawn on *in vivo* NIR fluorescence images. T/N ratios were derived from the MFI of ROIs and represented as Mean ± SD for all three groups (*n* = 10 per group). Comparisons of T/N ratios between the groups at 6 h *p.i.* and 24 h *p.i.* are shown on the right, ns: no significance, **P* < 0.05, ***P* < 0.01, ****P* < 0.001, *****P* < 0.0001. (e) Ex vivo fluorescence images of whole tumors resected at 24 h *p.i.* (f) The MFI of resected tumors at 24 h *p.i.* in different groups. Values represent Mean ± SD from six tumors per group (*n* = 6). (g) Bio-distribution of antibody conjugates in main organs and tumors resected at 24 h *p.i.* H, heart; Li, liver; Sp, spleen; Lu, lung; K, kidney; In, intestine; St, stomach; Mu, muscle; Bn, bone; Bl, blood; T, tumor. Values (Mean ± SD) are normalized to % injected dose/g (%ID/g) from three mice per group (*n* = 3). Only comparisons with *p* value less than 0.05 displayed, **P* < 0.05, ***P* < 0.001, *****P* < 0.0001.

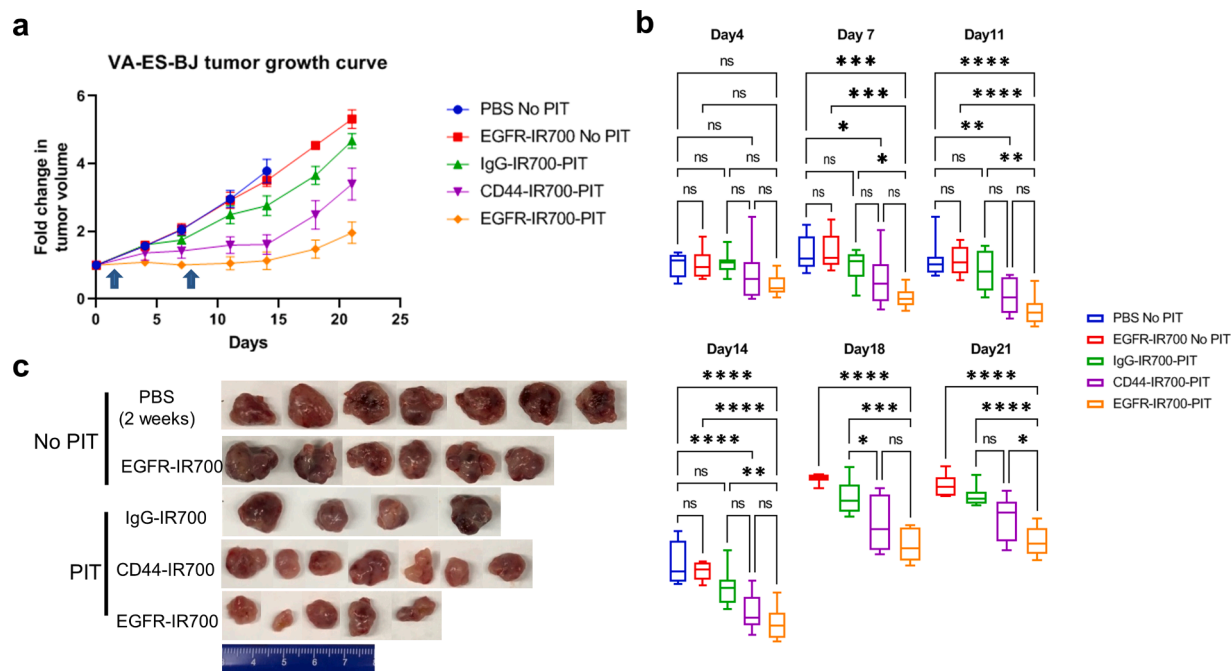


Fig. 4. In vivo CD44-IR700 or EGFR-IR700-PIT. (a) Growth curve of VA-ES-BJ tumors. 100 μ g of CD44-IR700 or EGFR-IR700 or IgG-IR700 was injected *i.v.* on day 0 and on day 7. All the groups were monitored for three weeks after injection except for two weeks in PBS group. PIT groups received light exposure at 200 J/cm², 24 h after each injection (pointed by blue arrows) and mice in the no PIT groups were shielded from light. Values represent Mean \pm SEM from at least four mice per group ($n \geq 4$). (b) The comparisons of tumor volumes between the groups at each monitoring point, ns: no significance, * $P < 0.05$, ** $P < 0.01$, *** $P < 0.001$, **** $P < 0.0001$. (c) Photographs of representative VA-ES-BJ tumors harvested at the end of treatment.

six days after PIT, tumor sizes in EGFR-IR700-PIT group were significantly smaller than those in the PBS, EGFR-IR700 No PIT, and IgG-IR700-PIT groups and continued to be significantly smaller throughout the entire monitoring period (Fig. 4b). Tumor growth arrest was evident in both CD44-IR700-PIT and EGFR-IR700-PIT groups until day 14, seven days after the repeat injection after which tumor volumes started to increase (Fig. 4a). These data suggest that the anti-tumor effects of both PITs lasted for approximately one week and then started to weaken if no repeated PIT was given. EGFR-IR700 injection alone did not show any effect on tumor growth with growth curves resembling the PBS group. IgG-IR700-PIT tended to show a slight anti-tumor effect in terms of the growth curve, but there were no significant differences in tumor volumes compared to the PBS group at all time-points (Fig. 4b).

Tumors from all the groups were resected at the end of treatment and representative excised tumors were photographed for documentation. Consistent with the growth curves in Fig. 4a, end-point tumor sizes in the CD44-IR700-PIT group were smaller than the ones in the PBS and

IgG-IR700-PIT groups; tumor sizes from the EGFR-IR700 group were even smaller as compared to the PBS, IgG-IR700-PIT and EGFR-IR700 No PIT groups (Fig. 4c). A slight weight loss was observed in all of the groups, but no significant difference was found between the groups at any time-point (Fig. S2). Some tumors in the CD44-IR700-PIT group did show slight skin scarring after NIR light exposure (data not shown) due to the expression of CD44 by epithelial cells in the skin.

CD44-IR700-PIT and EGFR-IR700-PIT reduce CD44 and EGFR levels in VA-ES-BJ tumors

To investigate the molecular changes caused by PIT, tumors were harvested three days after PIT and at the end of treatment to determine intermediate and end-point effects, using western blotting and flow cytometry. PIT reduced the total amounts of both CD44 and EGFR in tumors excised on three days after PITs irrespective of the antibody used as observed in the immunoblots (Fig. 5a). The percentage of CD44 and

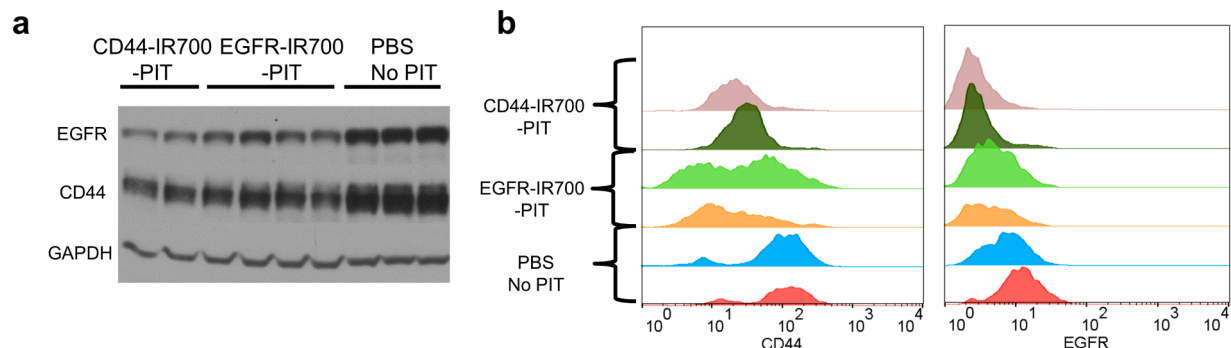


Fig. 5. Short-term effects of PIT on CD44 and EGFR. (a) Immunoblots probing CD44 and EGFR protein in VA-ES-BJ tumors. (b) Representative flow cytometry profiles of CD44 and EGFR expression in tumors after receiving PITs. 100 μ g of CD44-IR700 or EGFR-IR700 or 100 μ l of PBS was injected *i.v.* PIT groups received light exposure at 200 J/cm² 24 h after injection and mice in the PBS group were shielded from light. VA-ES-BJ tumors were harvested three days after single PIT. Tumors were dissociated into a single cell suspension and only live cells were included in the flow cytometry analysis.

EGFR-expressing cells relative to the total number of live cells obtained from dissociated tumors also decreased as detected by flow cytometry (Fig. 5b). These results suggest that CD44 and EGFR are both expressed on the same population of VA-ES-BJ cells; PIT-induced cell death resulted in a reduction of these proteins irrespective of the targeting antibody used. In the end-point tumors, CD44-IR700-PIT did not result in a decrease of CD44 and EGFR compared to the PBS group consistent with the lower effectiveness of CD44-IR700-PIT (Fig. S3). Consistent with the increased effectiveness of EGFR-IR700-PIT in vivo and the sustained growth delay compared to CD44-IR700-PIT, both CD44 and EGFR remained low in the end-point tumors from the EGFR-IR700-PIT group compared to the PBS group (Fig. S3).

Discussions

ES is a malignant STS with uncertain differentiation according to the 2020 WHO classification of tumors. Approximately 90 % of both classic and proximal ES show a complete nuclear loss of integrase interactor 1 (INI1) that is used to support the diagnosis of ES with immunohistochemistry [2]. To perform NIR-PIT of ES we investigated other mesenchymal and epithelial markers located on the plasma membrane, such as MUC1, CD44 and EGFR [4,41]. Our flow cytometry data showed that although MUC1 was overexpressed, it was the least abundant, leading us to select CD44 and EGFR for NIR-PIT.

In another study aimed at developing targeted therapies for ES, EGFR overexpression and activation was validated, and EGFR blockade alone showed promising responses in a preclinical ES model [42]. However, a phase 2 clinical trial utilizing cetuximab (EGFR monoclonal antibody) for the treatment of metastatic or locally advanced bone and soft tissue sarcomas failed [43]. This clinical study concluded that cetuximab was not active as a single agent in advanced sarcoma [43]. These findings are in agreement with our observation of no anti-tumor effect with EGFR-IR700 injection alone and highlight the necessity of introducing a therapeutic component into this targeted therapy regime such as the photosensitizer IR700 in our study.

Both CD44 and EGFR were expressed by VA-ES-BJ cancer cells. CD44 expression was observed in all four human ES samples and EGFR expression in three out of four human ES samples. The higher CD44 expression level of VA-ES-BJ cells resulted in a lower EC₅₀ value of CD44-IR700 in cellular PIT. In vivo, EGFR-IR700 exhibited higher retention in VA-ES-BJ tumors and a higher anti-tumor growth effect with PIT when compared to CD44-IR700-PIT, highlighting the importance of in vivo tumor validation studies. In human samples, CD44 was present on lymphocytes and cancer associated fibroblasts as well as cancer cells, whereas EGFR was located primarily on the cancer cells. These findings are consistent with CD44 being expressed by epithelial cells, bone marrow, and lymphoid tissue [39], and EGFR being mostly upregulated and activated in epithelial malignancies [44]. Collectively these findings suggest that EGFR may be a more effective target than CD44 in applications to manage ES with NIR-PIT.

Here, for the first time, we investigated the use of NIR-PIT in the management of ES with NIR-PIT using the VA-ES-BJ xenograft model. Future studies should focus on validating the target expression in a larger cohort of patient samples. NIR-PIT with patient-derived tumor samples will further validate applying NIR-PIT in eliminating cancer cells in tumor margins and as adjuvant therapy in combination with established treatments. For example, NIR-PIT can be used as a neoadjuvant therapy to facilitate radical resection, or as an adjuvant therapy to supplement or replace RT in the management of ES patients with positive margins after surgery, or as a palliative therapy for unresectable and metastatic ES. NIR-PIT can be expanded to include STS of the extremities, or locations such as the body wall, or head/neck that are accessible with NIR light. The NIR fluorescence of IR700 can be integrated into fluorescence-guided surgery to achieve clear margins, which may be of benefit for STSs with infiltrative histologies, such as myxofibrosarcoma, dermatofibrosarcoma protuberans, and angiosarcoma.

Ethical standards

All procedures involving humans were in accordance with the ethical standards of the national responsible committee on human experimentation and with the Helsinki Declaration of 1964 and later versions. The human pathology specimens were de-identified. All animal studies were conducted under an Animal Care and Use Committee approved protocol.

CRedit authorship contribution statement

Jiefu Jin: Writing – review & editing, Writing – original draft, Visualization, Validation, Methodology, Investigation, Formal analysis, Data curation, Conceptualization. **James D. Barnett:** Investigation, Data curation. **Yelena Mironchik:** Investigation, Data curation. **John Gross:** Writing – review & editing, Resources. **Hisataka Kobayashi:** Writing – review & editing, Resources, Methodology, Conceptualization. **Adam Levin:** Writing – review & editing, Resources, Conceptualization. **Zaver M. Bhujwala:** Writing – review & editing, Visualization, Supervision, Resources, Project administration, Funding acquisition, Conceptualization.

Declaration of competing interest

The authors declare that they have no known competing financial interests or personal relationships that could have appeared to influence the work reported in this paper.

Acknowledgments

This work was supported by NIH R35 CA209960, R01 CA82337, P41 EB024495, and P30 CA006973. We thank Dr. John Gross for generously providing human ES patient samples. We thank Dr. K. M. Horton for her support.

Supplementary materials

Supplementary material associated with this article can be found, in the online version, at [doi:10.1016/j.tranon.2024.101966](https://doi.org/10.1016/j.tranon.2024.101966).

References

- [1] F.M. Enzinger, Epithelioid sarcoma. A sarcoma simulating a granuloma or a carcinoma, *Cancer* 26 (5) (1970) 1029–1041.
- [2] K. Thway, et al., Epithelioid sarcoma: diagnostic features and genetics, *Adv. Anat. Pathol.* 23 (1) (2016) 41–49.
- [3] M.U. Jawad, et al., Prognostic factors for survival in patients with epithelioid sarcoma: 441 cases from the SEER database, *Clin. Orthop. Relat. Res.* 467 (11) (2009) 2939–2948.
- [4] J. Persitz, et al., Epithelioid sarcoma of the hand: a wolf in sheep's clothing, *J. Plast. Surg. Hand Surg.* 55 (2) (2021) 96–104.
- [5] P.S. Wolf, et al., Epithelioid sarcoma: the University of Washington experience, *Am. J. Surg.* 196 (3) (2008) 407–412.
- [6] S.T. Elsamna, et al., Epithelioid sarcoma: half a century later, *Acta Oncol.* 59 (1) (2020) 48–54.
- [7] A.M. Czarnecka, et al., Epithelioid sarcoma—from genetics to clinical practice, *Cancers (Basel)* 12 (8) (2020) 2112.
- [8] S.A. de Visscher, et al., Epithelioid sarcoma: still an only surgically curable disease, *Cancer* 107 (3) (2006) 606–612.
- [9] M. von Mehren, et al., Soft tissue sarcoma, version 2.2022, NCCN clinical practice guidelines in oncology, *J. Natl. Compr. Cancer Netw.* 20 (7) (2022) 815–833.
- [10] P.W. Pisters, et al., Analysis of prognostic factors in 1,041 patients with localized soft tissue sarcomas of the extremities, *J. Clin. Oncol.* 14 (5) (1996) 1679–1689.
- [11] C. Kim, et al., Different subtypes of epithelioid sarcoma and their clinical implication: long-term multi-institutional experience with a rare sarcoma, *Apmis* 125 (3) (2017) 223–229.
- [12] M. Gounder, et al., Tazemetostat in advanced epithelioid sarcoma with loss of INI1/SMARCB1: an international, open-label, phase 2 basket study, *Lancet Oncol.* 21 (11) (2020) 1423–1432.
- [13] N. Simeone, et al., Tazemetostat for advanced epithelioid sarcoma: current status and future perspectives, *Future Oncol.* 17 (10) (2021) 1253–1263.
- [14] S. Stacchiotti, et al., Safety and efficacy of tazemetostat, a first-in-class EZH2 inhibitor, in patients (pts) with epithelioid sarcoma (ES) (NCT02601950), *J. Clin. Oncol.* 37 (15, suppl) (2019) 11003.

- [15] M. Mitsunaga, et al., Cancer cell-selective in vivo near infrared photoimmunotherapy targeting specific membrane molecules, *Nat. Med.* 17 (12) (2011) 1685–1691.
- [16] R. Katsube, et al., Fibroblast activation protein targeted near infrared photoimmunotherapy (NIR PIT) overcomes therapeutic resistance in human esophageal cancer, *Sci. Rep.* 11 (1) (2021) 1693.
- [17] K. Sato, et al., Spatially selective depletion of tumor-associated regulatory T cells with near-infrared photoimmunotherapy, *Sci. Transl. Med.* 8 (352) (2016) 352ra110.
- [18] K. Sato, et al., Photoinduced ligand release from a silicon phthalocyanine dye conjugated with monoclonal antibodies: a mechanism of cancer cell cytotoxicity after near-infrared photoimmunotherapy, *ACS Cent. Sci.* 4 (11) (2018) 1559–1569.
- [19] H. Kobayashi, P.L. Choyke, Near-infrared photoimmunotherapy of cancer, *Acc. Chem. Res.* 52 (8) (2019) 2332–2339.
- [20] T. Nagaya, et al., Near infrared photoimmunotherapy targeting EGFR positive triple negative breast cancer: optimizing the conjugate-light regimen, *PLoS One* 10 (8) (2015) e0136829.
- [21] Y. Nakamura, et al., Near infrared photoimmunotherapy in a transgenic mouse model of spontaneous epidermal growth factor receptor (EGFR)-expressing lung cancer, *Mol. Cancer Ther.* 16 (2) (2017) 408–414.
- [22] M. Amoury, et al., Photoimmunotheranostic agents for triple-negative breast cancer diagnosis and therapy that can be activated on demand, *Oncotarget* 7 (34) (2016) 54925–54936.
- [23] D. Bauerschlag, et al., Detection and specific elimination of EGFR+ ovarian cancer cells using a near infrared photoimmunotheranostic approach, *Pharm. Res.* 34 (4) (2017) 696–703.
- [24] T.A. Burley, et al., Near-infrared photoimmunotherapy targeting EGFR—Shedding new light on glioblastoma treatment, *Int. J. Cancer* 142 (11) (2018) 2363–2374.
- [25] K. Sato, et al., Near infrared photoimmunotherapy for lung metastases, *Cancer Lett.* 365 (1) (2015) 112–121.
- [26] K. Takahashi, et al., HER2 targeting near-infrared photoimmunotherapy for a CDDP-resistant small-cell lung cancer, *Cancer Med.* 10 (24) (2021) 8808–8819.
- [27] T. Nagaya, et al., Near-infrared photoimmunotherapy targeting prostate cancer with prostate-specific membrane antigen (PSMA) antibody, *Mol. Cancer Res.* 15 (9) (2017) 1153–1162.
- [28] A.A. Maawy, et al., Near infra-red photoimmunotherapy with anti-CEA-IR700 results in extensive tumor lysis and a significant decrease in tumor burden in orthotopic mouse models of pancreatic cancer, *PLoS One* 10 (3) (2015) e0121989.
- [29] N. Shirasu, et al., Potent and specific antitumor effect of CEA-targeted photoimmunotherapy, *Int. J. Cancer* 135 (11) (2014) 2697–2710.
- [30] J. Jin, et al., Phototheranostics of CD44-positive cell populations in triple negative breast cancer, *Sci. Rep.* 6 (1) (2016) 27871.
- [31] J. Jin, et al., PD-L1 near infrared photoimmunotherapy of ovarian cancer model, *Cancers* 14 (3) (2022) 619.
- [32] S. Taki, et al., Spatiotemporal depletion of tumor-associated immune checkpoint PD-L1 with near-infrared photoimmunotherapy promotes antitumor immunity, *J. Immunother. Cancer* 9 (11) (2021) e003036.
- [33] J.D. Barnett, et al., Phototheranostics of splenic myeloid-derived suppressor cells and its impact on spleen metabolism in tumor-bearing mice, *Cancers* 14 (15) (2022) 3578.
- [34] J. Jin, et al., Evaluating near-infrared photoimmunotherapy for targeting fibroblast activation protein- α expressing cells in vitro and in vivo, *Cancer Sci.* 114 (1) (2023) 236–246.
- [35] S. Watanabe, et al., Photoimmunotherapy for cancer-associated fibroblasts targeting fibroblast activation protein in human esophageal squamous cell carcinoma, *Cancer Biol. Ther.* 20 (9) (2019) 1234–1248.
- [36] Y. Hiroshima, et al., Photoimmunotherapy inhibits tumor recurrence after surgical resection on a pancreatic cancer patient-derived orthotopic xenograft (PDOX) nude mouse model, *Ann. Surg. Oncol.* 22 (3) (2015) 1469–1474.
- [37] C. Chen, et al., The biology and role of CD44 in cancer progression: therapeutic implications, *J. Hematol. Oncol.* 11 (1) (2018) 64.
- [38] L.T. Senbanjo, M.A. Chellaiyah, CD44: a multifunctional cell surface adhesion receptor is a regulator of progression and metastasis of cancer cells, *Front. Cell Dev. Biol.* 5 (2017) 18.
- [39] E. Fernández-Tabanera, R.M. Melero-Fernández de Mera, J. Alonso, CD44 in sarcomas: a comprehensive review and future perspectives, *Front. Oncol.* 12 (2022) 909450.
- [40] M.J. Cascio, R.J. O'Donnell, A.E. Horvai, Epithelioid sarcoma expresses epidermal growth factor receptor but gene amplification and kinase domain mutations are rare, *Mod. Pathol.* 23 (4) (2010) 574–580.
- [41] C. Fisher, Epithelioid sarcoma of Enzinger, *Adv. Anat. Pathol.* 13 (3) (2006) 114–121.
- [42] X. Xie, et al., Combining EGFR and mTOR blockade for the treatment of epithelioid sarcoma, *Clin. Cancer Res.* 17 (18) (2011) 5901–5912.
- [43] H.T. Ha, et al., Phase II trial of cetuximab in patients with metastatic or locally advanced soft tissue or bone sarcoma, *Am. J. Clin. Oncol.* 36 (1) (2013) 77–82.
- [44] S. Kalyankrishna, J.R. Grandis, Epidermal growth factor receptor biology in head and neck cancer, *J. Clin. Oncol.* 24 (17) (2006) 2666–2672.